Electronic Supplementary Information

Specific Cu_2O surfaces for electrocatalytic oxygen reduction reaction

Chih-Chun Chang, Jui-Cheng Kao, Yu-Chieh Lo,* Jyh-Pin Chou*, Shang-Cheng Lin, Chun-Chia Wen, and Michael H. Huang*

Synthesis of Cu_2O cubes, octahedra, and rhombic dodecahedra. The specific reagent amounts used to synthesize these Cu_2O crystals are listed in Table S1. First, sodium dodecyl sulfate and deionized water were introduced to a beaker and stirred for about 5 min in a 31 ºC water bath. 0.1 M $CuCl_2$ solution was injected with vigorous stirring for 25 min. Next, 1.0 M NaOH solution was introduced. The solution color was immediately changed from colorless to light blue due to formation the $Cu(OH)_2$. After stirring for a few sec, 0.2 M $NH_2OH{\cdot}HCl$ solution was added quickly and stirred for 10–20 s. Then the mixture of solution was aged for 25–50 min. The product was collected by centrifugation at 10,000 rpm and washed with a 1:1 volume ratio of water and ethanol three times. Finally, the product was washed and preserved with 99.8 % ethanol.

Computational details. All the first-principles calculations based on the spin-polarized density functional theory were conducted by Vienna *ab initio* Simulation Package (VASP).[1,2] The projector augmented wave (PAW)[3] pseudopotential method, in combination with the Perdew–Burke–Ernzerhof (PBE)[4] functional within the generalized gradient approximation (GGA),[5] was selected to describe the exchange-correlation interaction. The cut-off kinetic energy for the plane-wave basis set was set to 480 eV, and the Brillouin zone (BZ) was sampled with 8 × 8 × 8 Γ-centered *k*-point grids for the Cu_2O primitive cell. The electronic convergence criterion was set to 10^{-5} eV. The optimized lattice constant is 4.30 Å, which is consistent with a previous experimental study.[6] The Cu_2O {100}, {110}, and {111} surfaces were modeled by the relaxed bulk primitive cell. The O-termination, CuO-termination, and stoichiometric termination were chosen to build for the {100}, {110}, and {111} surfaces displaying the lower surface energy.[7] The 3 × 3, 2 × 3, and 2 × 2 supercells were used to adsorb the reactant and intermediate products for the {100}, {110}, and {111} surfaces, respectively. The 3 × 3 × 1 *k*-point grids was sampled with the BZ for all the surface models. All the vacuum space along the surface normal is larger than 18 Å.

The adsorption energy (E_{ads}) was defined as

$$E_{ads} = E_{sys} - E_{O2} - E_{surf} \quad (1)$$

where E_{sys} and E_{surf} are the total energies of the surface model after and before adsorption, and E_{O2} is the total energy of the O_2 molecule. To investigate the ORR performance, the ORR reaction pathway was calculated according to the

computational hydrogen electrode (CHE) method developed by Nørskov and co-workers.[8] The overall reaction of ORR for the four-electron pathway in an alkaline electrolyte can be expressed as

$$O_2 + 2H_2O + 4e^- \leftrightarrow 4OH^- \quad (2)$$

The elementary steps involved in the ORR pathway follows:

$$O_{2(g)} + H_2O_{(l)} + e^- + {}^* \rightarrow OOH^* + OH^- \quad (3)$$

$$OOH^* + e^- \rightarrow O^* + OH^- \quad (4)$$

$$O^* + H_2O_{(l)} + e^- \rightarrow OH^* + OH^- \quad (5)$$

$$OH^* + e^- \rightarrow {}^* + OH^- \quad (6)$$

where *, OOH^*, O^*, and OH^* represent the active site on the catalyst surface and the corresponding three ORR intermediate products, respectively. The Gibbs free energy of each elementary steps can be written as

$$\Delta G = \Delta E_{DFT} + \Delta ZPE - T\Delta S + \Delta G_U \quad (7)$$

where ΔE_{DFT}, ΔZPE, and ΔS are changes in the calculated DFT energy, vibrational zero-point energy, and entropy, respectively. The temperature for the whole reaction step is set to 298.15 K. ΔG_U is the free energy change contributed by the bias effect, which is expressed

$$\Delta G_U = -neU \quad (8)$$

where U, e, and n are the electrode applied potential, the elementary charge transferred, and the number of proton–electron ($H^+ + e^-$) pairs transferred, respectively. Therefore, the reaction free energies of three ORR intermediates (ΔG_{OOH*}, ΔG_{O*}, ΔG_{OH*}) are evaluated by the free energy of stoichiometrically appropriate amounts of $H_2O_{(g)}$ and $H_{2(g)}$, and can be written as[9]

$$\Delta G_{OOH^*} = \left(E_{OOH^*} + 1.5E_{H_2} - 2E_{H_2O} - E_*\right) + \left(E_{ZPE(OOH^*)} + 1.5E_{ZPE(H_2)} - 2E_{ZPE(H_2O)} - E_{ZPE(} - T \times \left(S_{OOH^*} + 1.5S_{H_2} - 2S_{H_2O} - S_*\right) - 3eU \quad (9)$$

$$\Delta G_{O^*} = \left(E_{O^*} + E_{H_2} - E_{H_2O} - E_*\right) + \left(E_{ZPE(O^*)} + E_{ZPE(H_2)} - E_{ZPE(H_2O)} - E_{ZPE(^*)}\right) - T \times \left(S_{O^*} + \right. - 2eU \quad (10)$$

$$\Delta G_{OH^*} = \left(E_{OH^*} + 0.5E_{H_2} - E_{H_2O} - E_*\right) + \left(E_{ZPE(OH^*)} + 0.5E_{ZPE(H_2)} - E_{ZPE(H_2O)} - E_{ZPE(^*)}\right) - T \times \left(S_{OH^*} + 0.5S_{H_2} - S_{H_2O} - S_*\right) - eU \quad (11)$$

The entropy values of $H_2O_{(g)}$ and $H_{2(g)}$ at 298.15 K can be obtained through the NIST-JANAF thermodynamics tables.[10] Furthermore, the change in reaction free energy of the ORR pathway (ΔG_1, ΔG_2, ΔG_3, ΔG_4) are taken from the following equations:

$$\Delta G_1 = \Delta G_{OOH^*} - 4.92 \quad (12)$$

$$\Delta G_2 = \Delta G_{O^*} - \Delta G_{OOH^*} \quad (13)$$

$$\Delta G_3 = \Delta G_{OH^*} - \Delta G_{O^*} \quad (14)$$

$$\Delta G_4 = -\Delta G_{OH^*} \quad (15)$$

The theoretical limiting potential (U_L) and overpotential (η_{ORR}) are defined as

$$U_L = -max\{\Delta G_1, \Delta G_2, \Delta G_3, \Delta G_4\}/e \quad (16)$$

$$\eta_{ORR} = 1.23 - U_L \quad (17)$$

The higher limiting potential and lower overpotential represent an improved ORR activity.

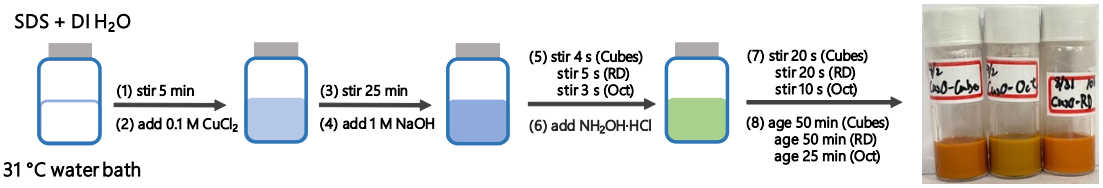

Fig. S1 Reaction conditions for making different Cu_2O polyhedra.

Table S1 Exact reagent amounts used to grow different Cu_2O polyhedra

	DI H_2O (mL)	SDS (g)	0.1 M $CuCl_2$ (mL)	1.0 M NaOH (mL)	NH_2OH·HCl (mL)
Cube	114.60	1.044	1.2	2.40	1.8 (0.2 M)
RD	27.68	0.348	2.0	0.72	9.6 (0.1 M)
Oct	26.20	0.348	0.8	0.80	2.6 (0.2 M)

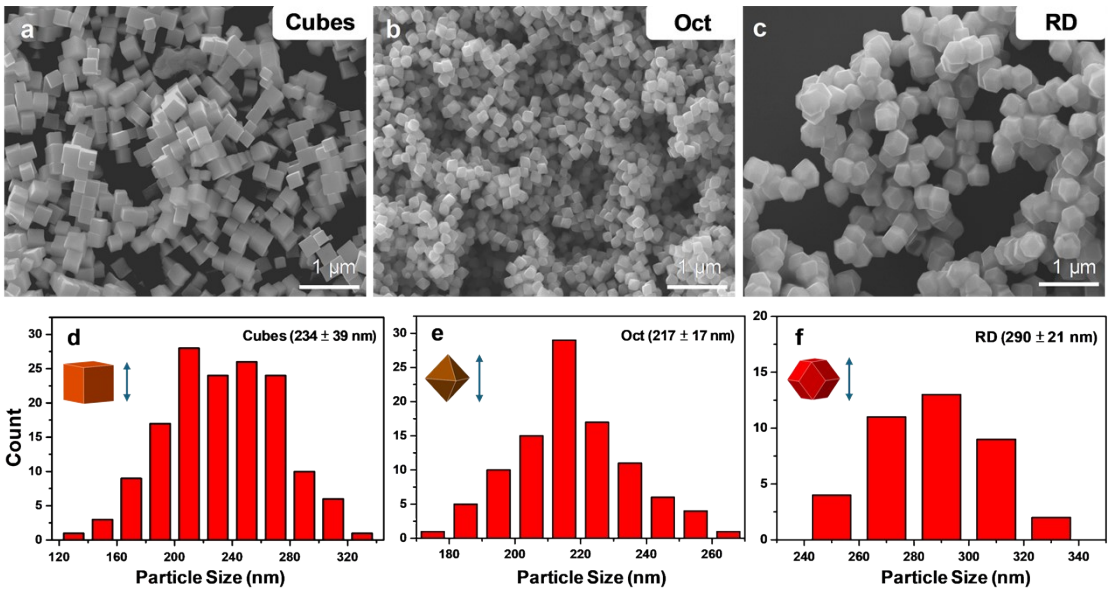

Fig. S2 (a–c) SEM images of the synthesized Cu_2O cubes, octahedra and rhombic dodecahedra. (d–f) Particle size distribution histograms of these particles.

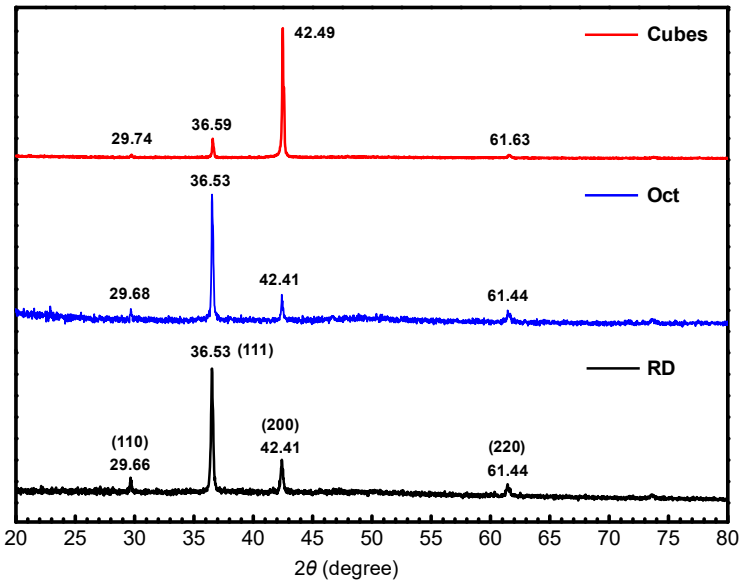

Fig. S3 XRD patterns of the synthesized Cu_2O crystals.

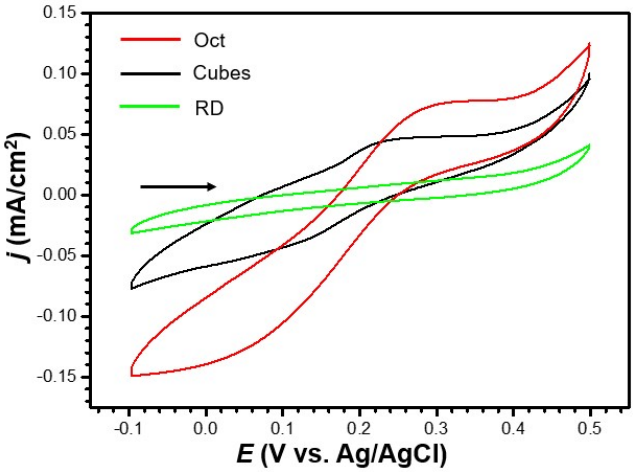

Fig. S4 Cyclic voltammetry curves of different Cu_2O crystals under 10 mV/s scan rate with 5 mM $K_3[Fe(CN)_6]$ in 0.1 M KCl electrolyte. The arrow indicates the scanning direction.

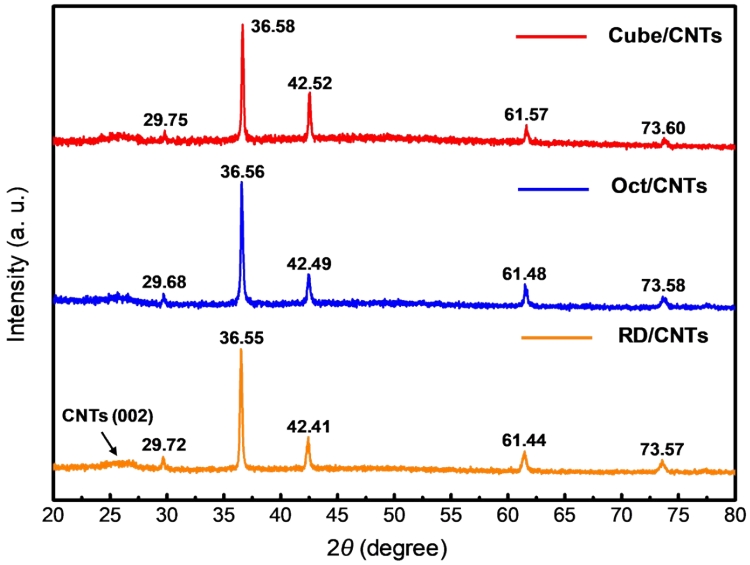

Fig. S5 XRD patterns of Cu_2O crystals in a CNT matrix.

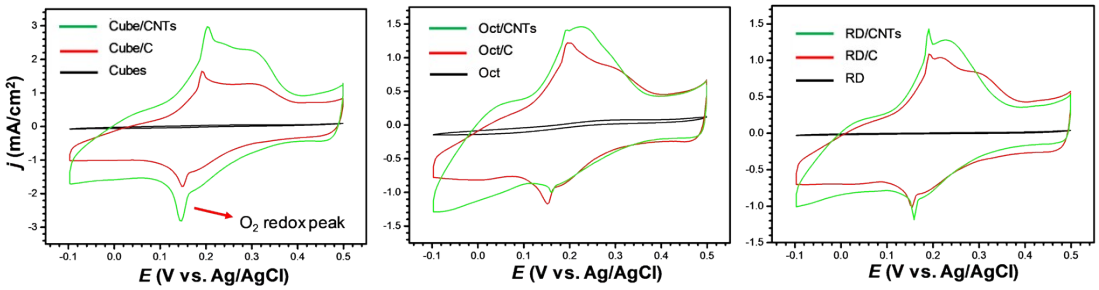

Fig. S6 Cyclic voltammetry curves of Cu_2O cubes, octahedra and rhombic dodecahedra with and without adding carbon powder and CNTs under a scan rate of 10 mV/s with 5 mM $K_3[Fe(CN)_6]$ in 0.1 M KCl electrolyte.

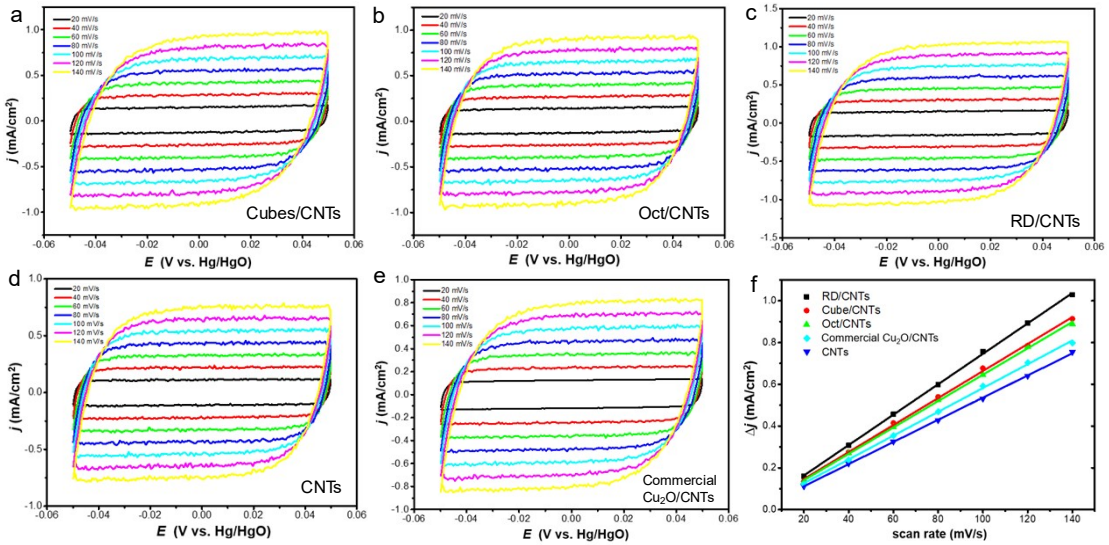

Fig. S7 (a–c) Cyclic voltammetry curves with different rotation rates for Cu_2O cubes, octahedra, and rhombic dodecahedra mixed with CNTs. (d, e) CV curves for CNTs and commercial Cu_2O mixed with CNTs. (f) The corresponding ECSA plot.

Table S2 ECSA-derived C_{dl} and C_{dl} ratios for different catalysts

	RD	Cubes	Oct	Commercial Cu_2O/CNTs	CNTs
C_{dl}	7.28	6.46	6.32	5.70	5.30
C_{dl} ratio	1.37	1.22	1.19	1.08	1

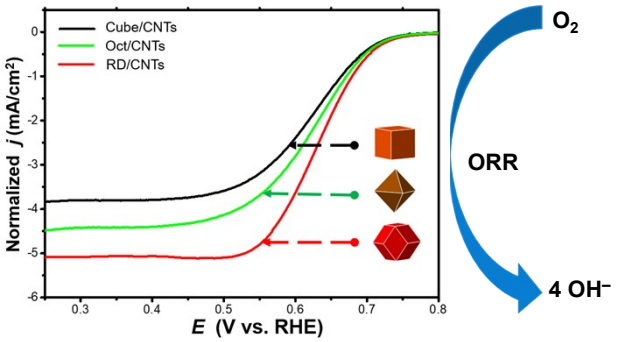

Fig. S8 LSV polarization curves for ORR in O_2-saturated 0.1 M KOH electrolyte at a scan rate of 5 mV/s and a rotating rate of 1600 rpm for the Cu_2O cubes/CNTs, octahedra/CNTs, and rhombic dodecahedra/CNTs.

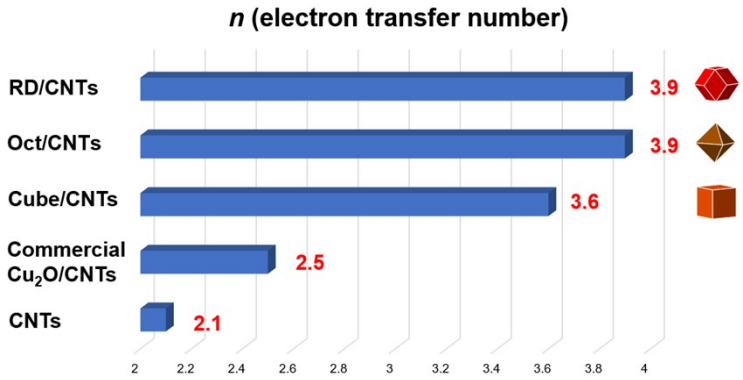

Fig. S9 Number of electrons transferred (n) in ORR for various catalysts.

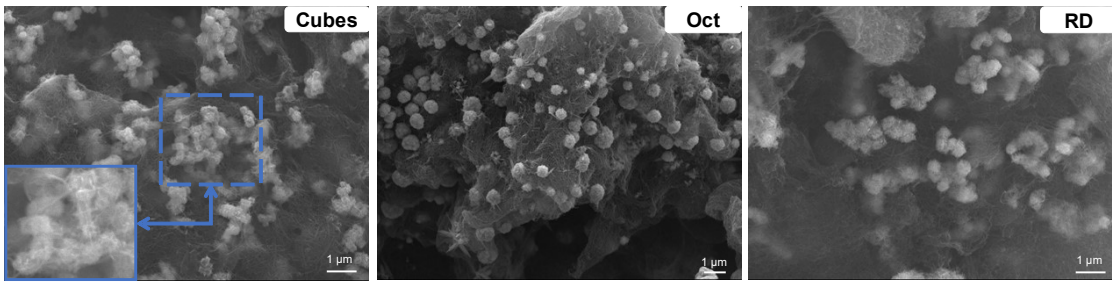

Fig. S10 SEM images of the Cu_2O/CNT catalysts after the chronoamperometric experiment.

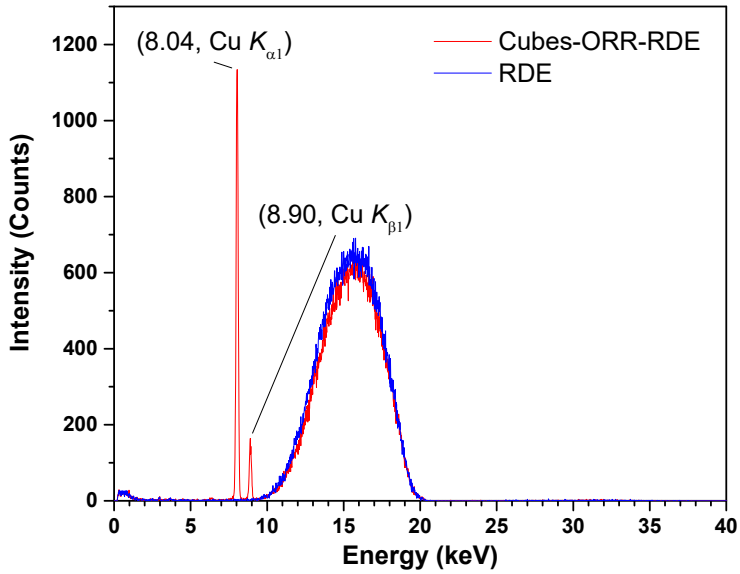

Fig. S11 X-ray fluorescence spectra of the rotating disk electrode and the Cu_2O cubes/CNT electrode after 6 h of ORR experiment under a constant potential of 0.65 V vs. RHE at a rotating rate of 1600 rpm in an O_2-saturated 0.1 M KOH solution. The background is a broad and intense peak between 10 and 20 keV. The large Cu $K_{\alpha 1}$ and Cu $K_{\beta 1}$ peaks are attributed to the Cu_2O crystals. No Pt signal was recorded, which should appear at 9.44 keV and 11.07 keV.

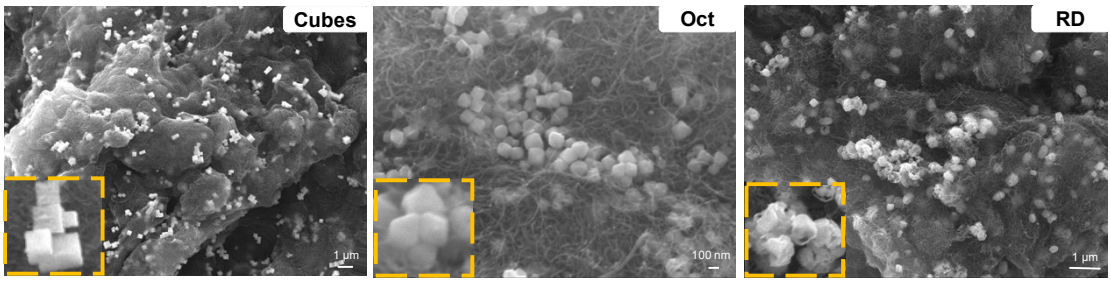

Fig. S12 SEM images of Cu_2O/CNT catalysts after storing at room temperature for two months.

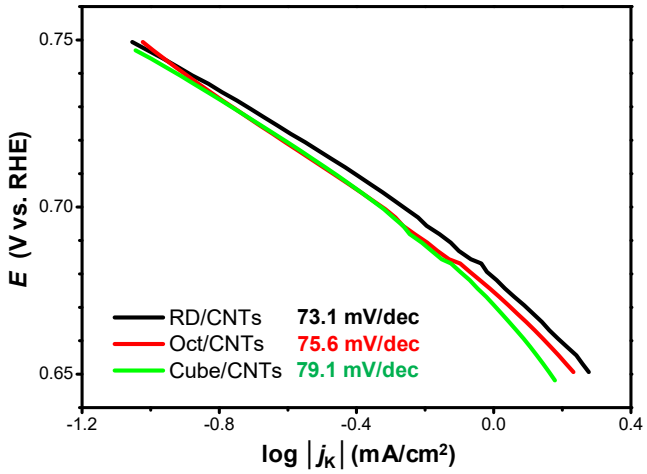

Fig. S13 Tafel plot of different Cu_2O crystals mixed with CNTs.

References

1 G. Kresse and J. Furthmüller, *Comput. Mater. Sci.*, 1996, **6**, 15–50.

2 G. Kresse and J. Furthmüller, *Phys. Rev. B*, 1996, **54**, 11169–11186.

3 P. E. Blöchl, *Phys. Rev. B*, 1994, **50**, 17953–17979.

4 J. P. Perdew, K. Burke and Y. Wang, *Phys. Rev. B*, 1996, **54**, 16533–16539.

5 J. P. Perdew, K. Burke and M. Ernzerhof, *Phys. Rev. Lett.*, 1996, **77**, 3865–3868.

6 A. Werner and H. D. Hochheimer, *Phys. Rev. B*, 1982, **25**, 5929–5934.

7 J.-C. Kao, J.-P. Chou, P.-J. Chen and Y.-C. Lo, *Mater. Today Phys.*, 2023, **38**, 101218.

8 J. K. Nørskov, J. Rossmeisl, A. Logadottir, L. Lindqvist, J. R. Kitchin, T. Bligaard and H. Jónsson, *J. Phys. Chem. B*, 2004, **108**, 17886–17892.

9 H. Xu, D. Cheng, D. Cao and X. C. Zeng, *Nat. Catal.*, 2018, **1**, 339–348.

10 NIST Standard Reference Database 13, NIST-JANAF Thermochemical Tables, https://janaf.nist.gov/, 2023.